Strathprints Institutional Repository

A note on threshold velocity criteria for modelling the solid particle erosion of WC/Co MMCs

B.D. Jana and M.M. Stack

Department of Mechanical Engineering,
University of Strathclyde,
James Weir Building,
75 Montrose St.,
Glasgow,
G3 6DD

1.0 Introduction

The purpose of this work has been to model the erosion of a metal matrix composite, by considering threshold criteria for erosion of the ductile and brittle phases of the composite, Figs. 1-2, in the composite, Fig. 3. In the literature, there has been some confusion on the effect of increasing reinforcement on the erosion of metal matrix composites MMCs [1-5]. Such effects are discussed in the context of the analysis of the model below and various trends observed for the solid particle erosion of metals and ceramics.

Early work on the erosion of WC/Co cermets showed a monotonic decrease in erosion rate with an increase in the volume fraction of reinforcement at normal impact at 133 ms^{-1} and with 10 μm silica particles [6], Fig. 4; in another study, for erosion of a similar material, at 40 ms^{-1} and with 100 μm SiC particles, the erosion rate increased up to a critical point whereupon it commenceμd to decrease again [7], Fig. 5. For the data, reported in [7], Fig. 6, the effect of impact angle showed that at lower values i.e. 15 and 30 degrees, a monotonic reduction in erosion with this variable was observed, thereby suggesting that as the normal component of velocity was increased (as is the case with an increase in impact angle), the trends in erosion with impact angle were reversed.

Considering, the erosion of ceramics and metals separately, some surprisingly similar observations have been made to the behaviour for metal matrix composites above.

For ceramics i.e. the erosion of soda lime glass, a monotonic increase in erosion with impact angle observed for larger particles sizes, Fig. 7, i.e. 21 μm, unlike the behaviour observed for the smaller 9 μm particles [8]. For erosion of mild steel for various particle compositions and sizes, Figs. 8-9, a reduction in erosion with increasing impact angle occurred for mild steel for impact with 50 μm angular SiC particles, Fig.8; whereas when the particle size was increased by a factor of 2 to 95-105 μm, using crushed glass beads as the erodent, a monotonic increase in erosion was observed [9], as a function of increasing impact angle. (In this study, the change in erosion behaviour was attributed to a perceived change in shape, citing the crushed glass particles as spherical and the SiC particles as angular in shape. However, the fact that the particle size was increased by a factor of two in the former case, was neglected in the analysis of the results.)

For MMCs, other studies have also observed such puzzling trends. In some cases, i.e. in the erosion of Ni-Cr-WC based MMCs, the addition of reinforcement particles resulted in a reduction in erosion rate up to a critical volume fraction. Above such volume fractions, an increase in erosion rate with increasing volume fraction was observed [10].

Such puzzling trends, for metallic and ceramic materials separately, have to some extent been addressed in the solid particle erosion literature through analysis of threshold effects of impact velocity and particle size on the erosion mechanism [11-16]. A threshold particle size for erosion of ductile materials was derived by Shewmon [11], where he pointed out that particles sizes below a nominal threshold value were incapable of removing material through plastic work. Lawn and co-workers [12-14], and Swain and Hagan [16] identified particle size as playing a key role in the indentation fracture mode of a brittle material. Impacting particles greater than 1 mm in diameter were thought to cause Hertzian cracking, whereas impacts below this size were thought to result in plastic deformation and formation of median cracks. In other work, Hutchings [17] generated erosion maps for ceramics, using threshold velocity criteria, and indicated the importance of particle size and velocity on the erosion rate transitions for these materials. However, what has not been

carried to date, is to use such threshold velocity criteria for the ductile and ceramic phases for an MMC to model the erosion behaviour.

In this paper, an analytical model for the threshold velocities for erosion of the ductile and brittle phases of a model metal matrix composite system, WC/Co, impacted by 0.1 mm SiC particles was developed. Models for the erosion rates above and below the threshold velocities for erosion of the Co and WC reinforcements were also established. The models derived show agreement, albeit qualitative, with some of the puzzling trends in the erosion results of WC/Co reported in the literature, as described above.

2.0 Development of mathematical model

2.1 Threshold velocity of an indenting particle to cause plastic deformation of ductile materials

In solid particle erosion of materials, threshold velocities depicting the onset to plastic damage of the material have been identified [17]. For the threshold velocity calculation, a Hertzian analysis was used [18] based on schematic representation of the impact event at 90^o in Fig. 1.

The radius of the indentation, a, formed for impact (assumed to be elastic) of a sphere on a ductile material sample can be given as

$$a = \left(\frac{3}{4} pKR_b\right)^{\frac{1}{3}} \qquad 1$$

where p is the load exerted by the spherical erodent on the material surface, R_b is the radius of the sphere and

$$K = \frac{1 - \upsilon_b^2}{E_b} + \frac{1 - \upsilon_{D/M}^2}{E_{D/M}} \qquad 2$$

where the values of Poisson's ratio and elastic modulus for both the spherical erodent and the ductile matrix are given by ν_b and $\nu_{D/M}$ and E_b and $E_{D/M}$ respectively.

The distance of mutual approach of the ball and the sample, h, can be given as

$$h = \left(\frac{9}{16} \frac{p^2 K^2}{R_b}\right)^{\frac{1}{3}} \qquad 3$$

According to the analysis of Timoshenko and Goodier [19], the maximum depth (α_m), the erodent sphere can penetrate into the ductile substrate can be calculated as:

$$\alpha_m = \left(\frac{5}{4} \frac{mV^2}{n} \right)^{\frac{2}{5}} \quad 4$$

where, m and V are the mass and the velocity of the erodent ball, and

$$n = \left(\frac{16}{9} \frac{R_b}{K^2} \right)^{\frac{1}{2}} \quad 5$$

The maximum compressive force (P_m) exerted by the sphere on the ductile substrate is estimated from equation 3 and 4, as follows:

$$P_m = 3.03 R_b^2 \rho_b^{\frac{3}{5}} V^{\frac{6}{5}} K^{-\frac{2}{5}} \quad 6$$

The maximum area of indentation (A_m) under the maximum load (P_m) can be calculated from equation 1 and 6, as follows:

$$A_m = 1.31 R_b \rho_b^{\frac{1}{5}} V^{\frac{2}{5}} K^{\frac{1}{5}} \quad 7$$

According to Tabor [20], the maximum mean pressure (dividing equation 6 by equation 7) is the static hardness of the ductile/matrix substrate ($H_{D/M}$).

Hence:

$$P_m/A_m = H_{D/M} \quad 8$$

A similar attempt was made to calculate maximum pressure for Hertzian fracture by Davies [18]

From equation 8, the threshold velocity ($V_{D/M}$) for the plastic deformation of the ductile substrate can be calculated and is given as:

$$V_{D/M} = 4.3 H_{D/M}^{\frac{5}{2}} K^2 \rho_b^{-\frac{1}{2}} \quad 9$$

2.2 Threshold velocity for an indenting particle to cause lateral cracking of ceramic materials

As in the case of a sharp particle indentation, where the load is concentrated at a point, a small spherical particle (less than 1mm size) indentation on a brittle ceramic substrate can also deform the substrate plastically [11, 16]. This so-called plastic deformation of ceramic may occur due to plastic flow or structural densification [21]. A schematic representation of the impact event is given in Fig. 2. During loading of the indentation process, a small spherical indenter impact may produce a plastically deformed zone beneath the impression and, at a critical threshold velocity, a median crack nucleates at the elastic/plastic interface and grows further with further loading.

During unloading, the median crack closes whereupon lateral cracks, extending outwards from the crack tip, commence to form. In this work, we considered the threshold velocity for the nucleation of the median crack, as this velocity is much less than the velocity required for the lateral crack formation.

Following the analysis of Lawn and Evans [13] and considering a spherical instead of sharp indenter, the threshold load for median crack nucleation can be given as:

$$P_o = 3.4 \times 10^4 K_{IC}^4 H_{B/R}^{-3} \qquad 10$$

where K_{IC} and $H_{B/R}$ are the mode-I fracture toughness and static hardness of the brittle/reinforcing material respectively.

The radius of the indentation, a_c, formed by the impact of the spherical erodent on the ceramic substrate can be given as [16]

$$a_c = 2^{1/2} R_b V^{1/2} \left(\frac{2\rho_b}{3H_{B/R}} \right)^{1/4} \qquad 11$$

where V is the velocity of the indenting ball.

The indentation force required for the crater (of radius a_c) formation can be given as:

Indentation force = $\pi a_c^2 H_{B/R}$ 12

For median crack nucleation, the indentation force has to be equal or greater than the threshold load required for median crack nucleation. Based on this analogy, the threshold velocity ($V_{B/R}$) for the median crack nucleation can be calculated from equation 10-12, as follows:

$$V_{B/R} = 6.63\times10^3 K_{IC}^4 H_{B/R}^{-7/2} R_b^{-2} \rho_b^{-1/2} \quad 13$$

Equation 9 and 13 are the expressions for the threshold velocities of indenting particle to initiate plastic deformation of ductile substrate and median crack on brittle/ceramic substrate respectively. Threshold velocities calculated using these two equations have been used to establish criteria for erosion of WC/Co cermets investigated. The criteria for erosion are outlined below.

2.3 Development of model for erosion of MMCs

2.3.1 Criteria for erosion

For erosion of composite materials, the total erosion is the sum of the component values of the matrix, the reinforcing phase and the interface between the two phases. Whether the matrix, the reinforcement or both materials together contribute to the total wastage of the MMC can be determined by estimating the individual threshold velocities for erosion of the individual ductile and brittle phases. (The erosion of the interface is neglected in this analysis- this will be addressed further below). The following criteria are then used to assess which erosion mechanisms predominate:

$V \leq V_{D/M}$ no erosion (both matrix and reinforcement absorb the impact energy through elastic work)

$V_{D/M} < V \leq V_{B/R}$ total erosion is due to that of the matrix only

$V > V_{B/R}$ total erosion is due to that of the matrix and reinforcement

Such criteria can effectively be used for a particulate MMC (assuming a strong interfacial bond between the matrix and the reinforcement) so that during the erosion process, no particle becomes dislodged from the matrix. (It should be noted that the assumption that particles will not dislodge at higher impact energies is a simplistic assumption; it is probable that at such impact energies some debonding at the particle/matrix interface will take place.)

For this work, the performance of a simple system, an WC/Co composite was considered with the erodent a spherical particle of SiC of 0.1mm diameter.

2.3.2 Outline of the model

The dimensionless erosion rate for a composite (ε_{comp}), Fig. 3, having mass fraction M_R of reinforcing phase can be derived from the inverse rule of mixture law [5] as follows:

$$\frac{1}{\varepsilon_{comp}} = \frac{1 - M_R}{\varepsilon_M} + \frac{M_R}{\varepsilon_R} \qquad 14$$

where ε_M and ε_R are the dimensionless erosion of the matrix and reinforcement respectively. The erosion rate of the composite and other phases are considered as (mass/mass unit) and M_R can be correlated with the volume fraction of the reinforcing phase (F_R) by the following relationship:

$$M_R = \frac{F_R \rho_R}{\rho_{comp}} \qquad 15$$

where ρ_R and ρ_{comp} are the density of reinforcing phase and composite respectively.

The dimensionless erosion of the ductile matrix (ε_M) at normal impact can be represented by the model derived by Sundararajan and Shewmon [22] as follows:

$$\varepsilon_M = \frac{6.5X10^{-3} \rho_b^{0.25} V^{2.5}}{C_p T_m^{0.75} H_{D/M}^{0.25}} \qquad 16$$

where ρ_b is the density of the erodent ball, V is the velocity of the particle. C_P, T_m and $H_{D/M}$ are the specific heat, melting point and static hardness of the matrix material respectively.

For a brittle material, there are various models for the prediction of the erosion rate. However, a quasi-static model is considered in this work and thus the dimensionless erosion of a ceramic surface by a spherical erodent at normal incidence [23] can be given as:

$$\varepsilon_R = \rho_R H_{B/R}^{1/3} K_{IC}^{-4/3} R_b^{2/3} V^2 \qquad 17$$

Finally, the erosion rate of composite, in units of kg m^{-2} s^{-1}, is defined according to the following relationship

$$K_E = C V \varepsilon_{comp} \qquad 18$$

where K_E is the erosion rate of the MMC in kg m^{-2} s^{-1}, C and V are the concentration and velocity of slurry, and ε_{comp} is the dimensionless erosion rate of the MMC.

3.0 Results

The threshold velocity for the matrix (Co) and the reinforcement (WC) have been calculated using equation 9 and 13 respectively and have been presented in Table 1. Using the erosion criteria, presented in section 2.3.1, the erosion rate of WC/Co composite (in kg m^{-2} s^{-1}), for a range of impact velocities, has been calculated and plotted against the volume percent of WC content in the composite.

For impact at 10 and 20 ms^{-1}, Figures 10-11, the impact velocities were below the threshold velocities for erosion of WC. In this case, erosion of the ductile Co was the predominant erosion mechanism and thus additions of reinforcement particles caused an overall decrease in the predicted erosion rate as shown in Figures 10-11.

As the effects of debonding at the particle- matrix interface have been neglected in this study, it should be noted that erosion of the matrix (Co) was the predominant erosion process in this velocity range ie. 10 and 20 ms^{-1}, Figures 6-7. The results agree qualitatively with the evidence, Figure 4, found in the literature [6], where the

erodent impact velocity is above the threshold velocity for erosion of the matrix material, as defined by the model results, but well below the threshold velocity for erosion of the WC.

For impact at 30, 40 and 60 ms^{-1}, a diametrically opposite trend was observed, Figures 12-14. In this case, the threshold velocities for erosion of the Co and WC were exceeded at all three velocities. Hence, the inverse rule of mixtures model has been used to calculate the erosion rate of the composite system studied. The increase in predicted erosion rate with increasing volume fraction of WC, Figures 12-14, is in contrast to the trends observed at the lower velocities, Figures 10-11. This is attributable to the change in erosion mechanism, where both the matrix and reinforcement material erode simultaneously through ductile and brittle modes respectively.

4.0 Discussion

In the literature [1-7], as discussed above, there is little agreement on a mechanistic model for prediction of the erosion rate of MMCs. This is due to inconsistency of the mechanism of erosion of MMCs reported for various conditions as discussed above. Earlier work on testing of erosion of MMCs suggested the somewhat contradictory results in the literature above arise from the change in the erosion mechanism of the reinforcement, as shown above [2-4]. As long as cracking of the reinforcement particles can be avoided, additions of reinforcements to MMCs can reduce erosion. The model outlined above is a new attempt to explain the somewhat surprising and confusing trends on erosion rate with reinforcement volume fraction as observed in the literature [6-7], using material removal criteria based on threshold velocity for erosion of the matrix and reinforcement and therefore this is an important new development in erosion models for composite materials.

Table 1 indicates that impact velocities of 10 and 20 ms^{-1} respectively are well below the threshold velocities for erosion of WC. Hence, erosion of the cobalt matrix occurs only and the decreasing trend of erosion with increasing WC volume fraction, Figures.

10-11, is similar to that obtained in the literature for low impact energy erosion events on composites [2-4]. For velocities of 30- 60 ms^{-1}, Figures 12-14, the threshold conditions for both erosion of reinforcement and matrix material are satisfied. In this case, by contrast, a monotonic increase in the erosion rate with increasing reinforcement volume fraction is observed. This is similar to the increase in erosion with increasing reinforcement volume fraction [7], Figure 5, observed for the WC/Co system in other erosion conditions and suggests that, in this case, the reinforcement is providing no resistance to the eroding particles. Hence, the model can predict qualitatively two of the puzzling trends which have been observed for erosion of MMCs in the literature [6-7].

The model, however, does not predict the situation where more than one transition is observed in the erosion behaviour as a function of increasing reinforcement volume fraction i.e. the increase and subsequent decrease in erosion rate above a critical volume fraction as depicted in Figure 5 [7] for erosion of a WC/Co system at 90^{o}, or the reduction and subsequent increase in erosion rate, above and below a critical reinforcement volume fraction, as has been observed for erosion of the Ni-Cr-WC system [10]. In the former case, the reasons for such transitions may be due to the MMC acting as a homogenous rather than a heterogenous material, with the higher packing density at higher volume fractions promoting a more ductile response than at lower reinforcement volume fractions, thereby, as a result, identifying a further threshold effect based on distance between reinforcement particles. In the latter case, the behaviour is unexplained at present. What both sets of results do indicate, however, is that the scale of the erodent versus the reinforcement is important but to date such effects have not been considered in the analysis and it is clear from the model results and the literature results, presented above, that there are many other factors to be considered to extend the analysis.

Although the model above was generated for normal impact, the trends on impact angle for the both metallic and ceramic materials and MMCs, Figs. 6-9, would suggest that threshold impact angles may be identified for erosion of MMCs. This is an important parameter which could be incorporated in further model development. The size effect for erosion of ceramics has been addressed in previous work, Fig.7 [9]; but such effects are also observed for erosion of metallic materials, Figs. 8-9 [8]

suggesting that the trends in the results, Figs. 10-14, may also change for erosion with larger particles and as a result in change in threshold impact energies for the separate phases of the material.

The model has not taken account of particle/matrix debonding. However, in corrosive conditions, such sites may corrode preferentially leading to acceleration of the detachment of reinforcement particles from the matrix as defined on erosion-corrosion maps [27-29]. Further work will consider how the particle/matrix interface may affect the erosion mechanism as outlined above.

Although this study involves the erosion of MMCs, the trends discussed above may suggest a re-consideration of some trends in the solid particle erosion literature for both metallic and ceramic materials. "Ductile" and "brittle" erosion behaviour as a function of impact angle is often cited, as was originally envisaged, as a material response [30], but almost never as a relationship which may reverse if the threshold conditions for erosion of these materials are exceeded, as identified above, [8-9], despite much new erosion data emerging in recent years as discussed above. The results above suggest that some re-examination of the impact angle relationship in the solid particle erosion literature should be made based on the analysis of threshold effects for erosion of materials at various impact angles.

.

Hence, the model predictions account in a very qualitative manner for some of the differences in trends on the erosion rate of MMCs as found in the literature [1-7]. However, as indicated above, some but not all of the complex narrative regarding the erosion of MMCs is described by the model results. Further work will be to investigate the above areas in addition to assessing how such a model could apply to other composite systems.

5.0 Conclusions

(i) Using threshold velocity criteria for erosion of ductile and brittle materials, a model for erosion of metal matrix composites (MMCs) has been generated.

(ii) The basis of the erosion model is the establishment of critical velocity transitions for the onset of plastic deformation of the ductile matrix material and median crack formation of the brittle reinforcement.

(iii) The predictions from the model have shown qualitative agreement with some, but not all, of the trends observed for the solid particle erosion of MMCs in the literature.

6.0 References

1 N. Chawla and K.K. Chawla, Metal Matrix Composites, (2006), Springer, New York.

2 I.M. Hutchings: Proceedings of the 2nd European Conference on Advanced Materials and Processes, EUROMAT 91, ed. T.W. Clyne and P.J. Withers, Institute of Materials, London, 1962, pp. 56-64

3 I.M. Hutchings and A. Wang: Inst. of Physics Conf. Series- New Materials and their Applications, vol. 111, 1990, pp. 91-100

4 D.A.J Ramm, I.M. Hutchings and T.W. Clyne: Journal De Physique IV, 1993, vol. 3, pp. 913-919

5 S.K Hovis, J.E. Talia and R.O. Scattergood: Wear, 1986, vol. 108, pp. 139 – 155

6 I.G. Wright and D.K Shetty: Proc. 7th Int. Conf. on Erosion by Liquid and Solid Impact, Cavendish Laboratory, Cambridge, UK, 1987 paper 43

7 R.C. Pennefather, R. Hutchings and A. Ball: Proc. 7th Int. Conf. on Erosion by Liquid and Solid Impact, Cavendish Laboratory, Cambridge, UK, 1987 paper 60

8 G.L. Sheldon, Trans ASME B. Journal of Engineering for Industry, 88, 387-392, 1966.

9 A.K. Cousens and I.M. Hutchings, Proc. Erosion by Liquid and Solid Impact (ELSI 6), 5-8 September, Cambridge, 1983.

10 M.M. Stack and D. Peña, Wear 1997, vol 203-204, pp 489-497.

11 P.G. Shewmon: Wear, 1981, vol. 68, pp. 253-258

12 B.R. Lawn and R. Wilshaw: Journal of Materials Science, 1975, vol. 19, pp. 1049-1081

13 S.M. Wiederhorn and B.R. Lawn: Journal of the American Ceramic Society, 1977, vol. 60, pp. 451-458

14 B.R. Lawn and A.G. Evans: Journal of Materials Science, 1977, vol. 12, pp. 2195-2199

15 D.B. Marshall, B.R. Lawn and A.G. Evans: Journal of the American Ceramic Society, 1982, vol. 65, pp. 561-566

16 M.V. Swain and J.T. Hagan: Journal of Physics D- Applied Physics, 1976, vol. 9, pp. 2201-2214

17 I.M. Hutchings: Journal of Physics D- Applied Physics, 1992, vol. 25, pp. A212-A221

18 R.M. Davies: Proceedings of the Royal Society A, 1949, vol. 197, pp. 416-432

19 S. Timoshenko and J.N. Goodier: Theory of Elasticity, McGraw-Hill, New York, 1970

20 D. Tabor: The Hardness of Metals, The Clarendon Press, Oxford, 1951

21 B.R. Lawn and M.V. Swain: Journal of Materials Science, 1975, vol. 10, pp. 113-122

22 G. Sundararajan and P.G. Shewmon: Wear, 1983, vol. 84, pp. 237-258

23 M.R. Murugesh and R.O. Scattergood: Journal of Materials Science, 1991, vol. 26, pp. 5456-5466

24 G.J.C. Kaye and T.H. Laby: Tables of physical and chemical constants, 14th edition, Longman, New York, 1975, pp. 155-167

25 C.J. Smithells and E.A. Brandes: Metal Reference Book, 5th edition, Butterworth, London & Boston, 1976.

26 S.R. Lampman and T.B. Zorc: ASM Metals Handbook, 10th edition, vol. 2, Materials Park, OH, 1990.

27 M.M. Stack and B.D. Jana: Tribology International 2006, vol. 38, Issues 1-12, pp. 995-1006.

28 M.M. Stack, S.M. Abdelrahman and B.D. Jana, Wear 2010, vol 268, 3-4, pp 533-542.

29 M.M. Stack and T.M. Abd El Badia, Wear 2008, vol 264, pp 826-837

30. I.Finnie, J. Wolak and Y.H. Kabil, Journal of Mat., 2, 682-700, p1967

Figures

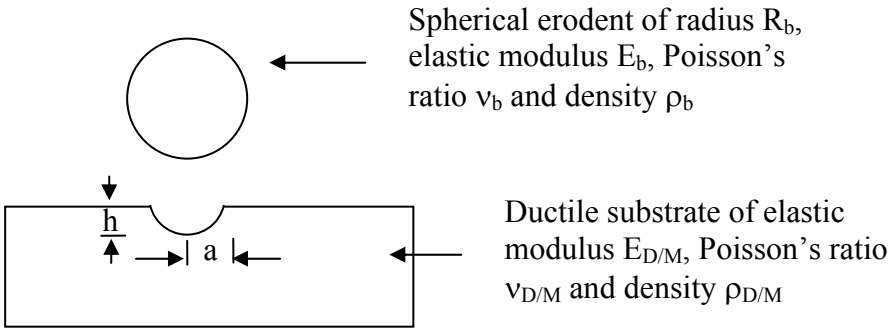

Fig. 1 Schematic diagram of an erosion event by a spherical indenter on a ductile surface

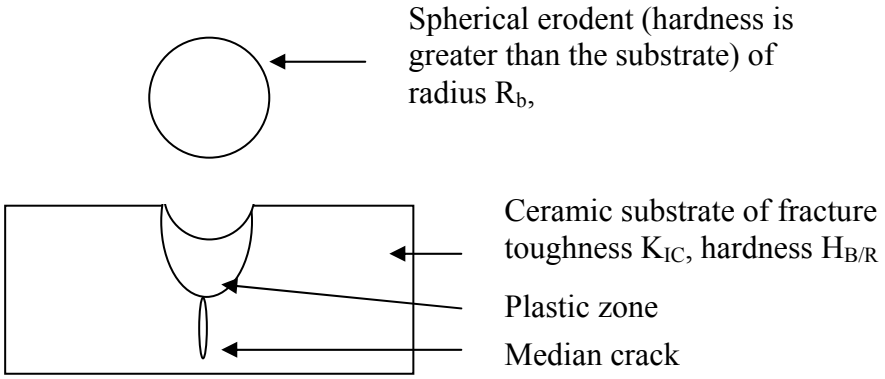

Fig. 2 Schematic diagram of an erosion event by a spherical indenter on a brittle substrate surface causing the formation of median cracks in the surface

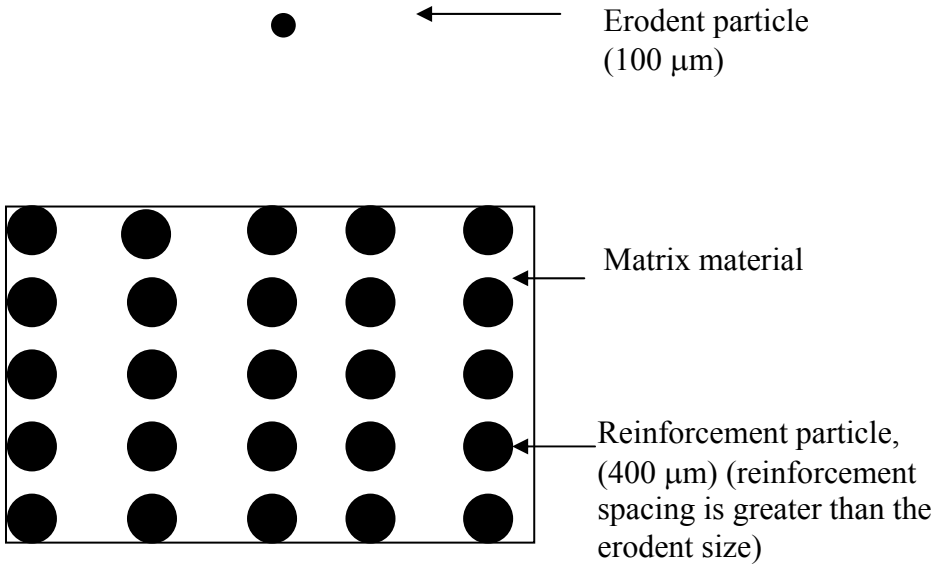

Fig. 3 Schematic diagram of the erosion processes of a particulate reinforced MMC as represented in the mathematical model

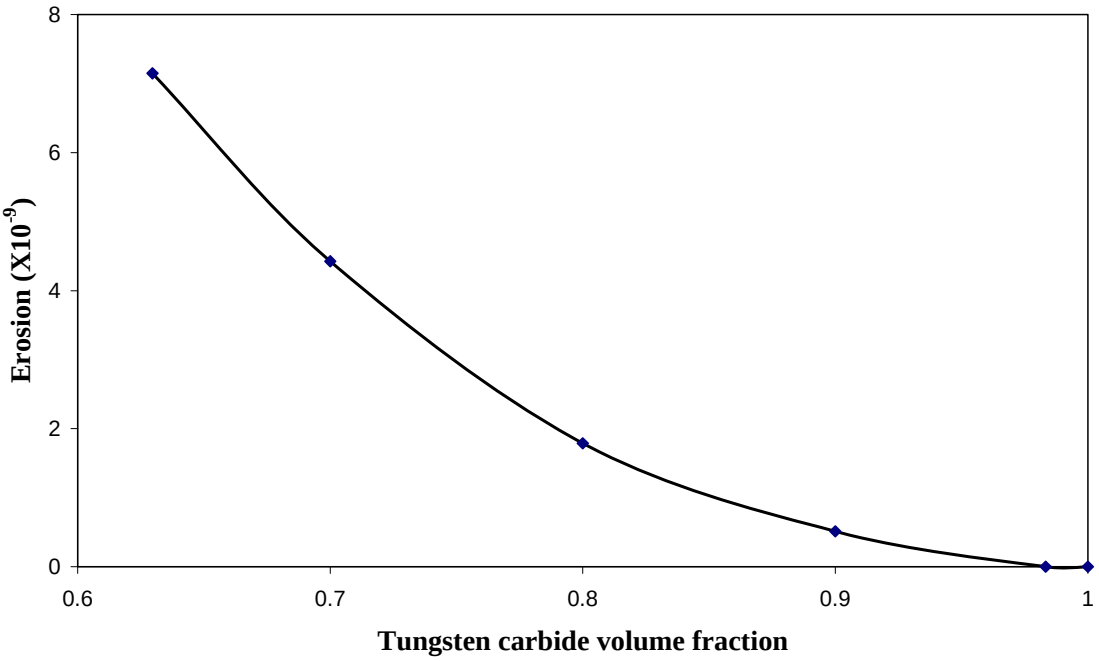

Fig. 4 Erosion rate versus volume fraction of WC for a WC-Co cermet, following impact by a slurry of 10 μm silica particles in oil at 133 ms^{-1} and impact angles of 90^o [6] (Threshold velocity for erosion of Co is 0.21 ms^{-1}, and WC is 2651.6 ms^{-1}, according equations 9 and 13 respectively)

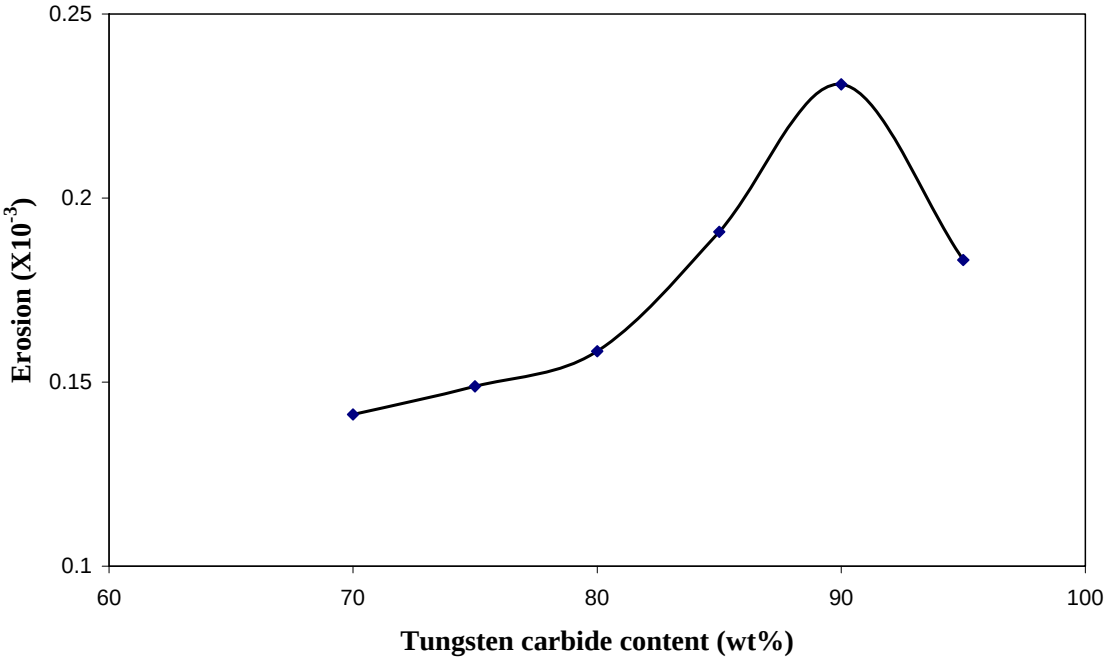

Fig. 5 Erosion rate versus WC content for a WC-Co cermet, following impact by a slurry of 100 μm silicon carbide particles at 40 ms^{-1} and at impact angles of 90^o [7] (Threshold velocity for erosion of Co is 0.21 ms^{-1},and WC is 26.52 ms^{-1}, according to equation 9 and 13 respectively)

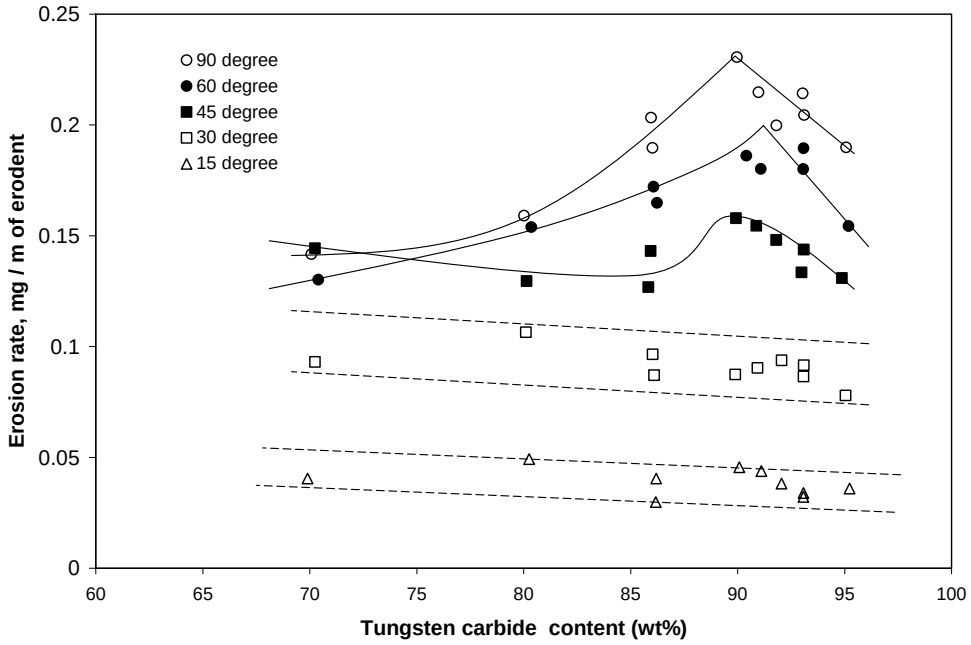

Fig. 6: Erosion rate as a function of WC carbide content for a number of incidence angles using 100 μm SiC particles [7]

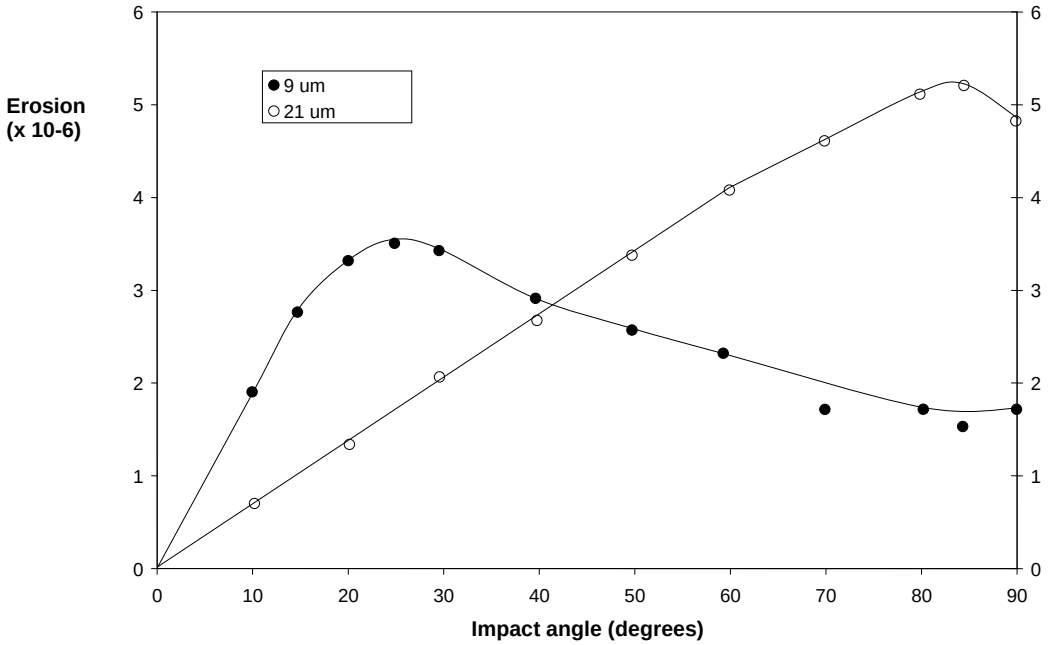

Fig. 7: Dependence of erosion rate on impact angle for soda lime glass eroded by 9 μm and 21 μm SiC particles at 136 ms^{-1} [9]

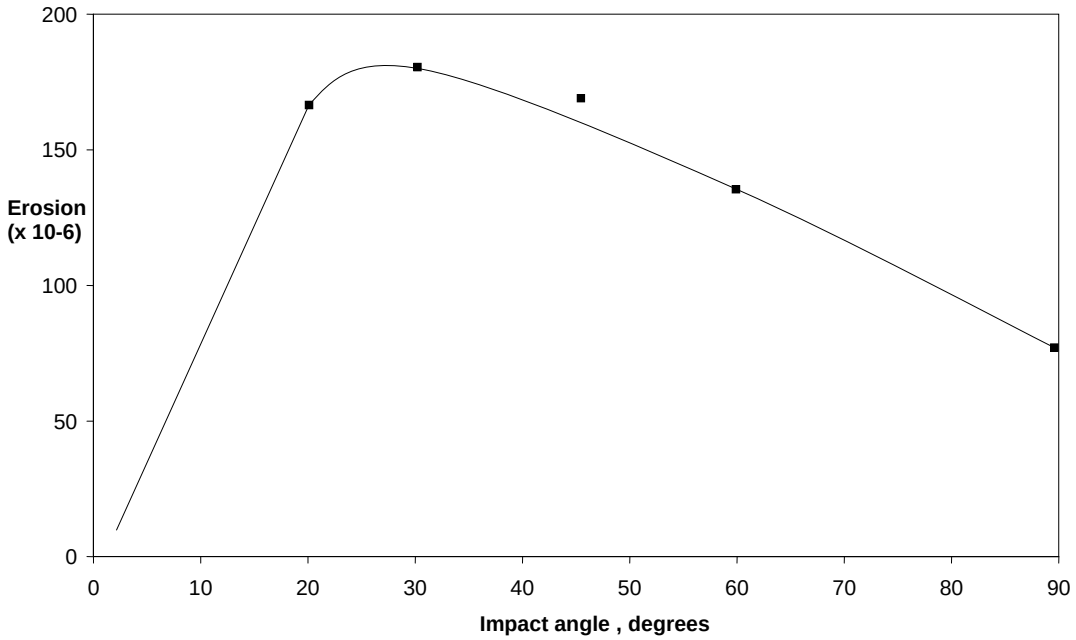

Fig. 8: Erosion as a function of impingement angle for angular SiC erodent (erodent size 280 mesh i.e. 50μm) at 55 ms^{-1} [8]

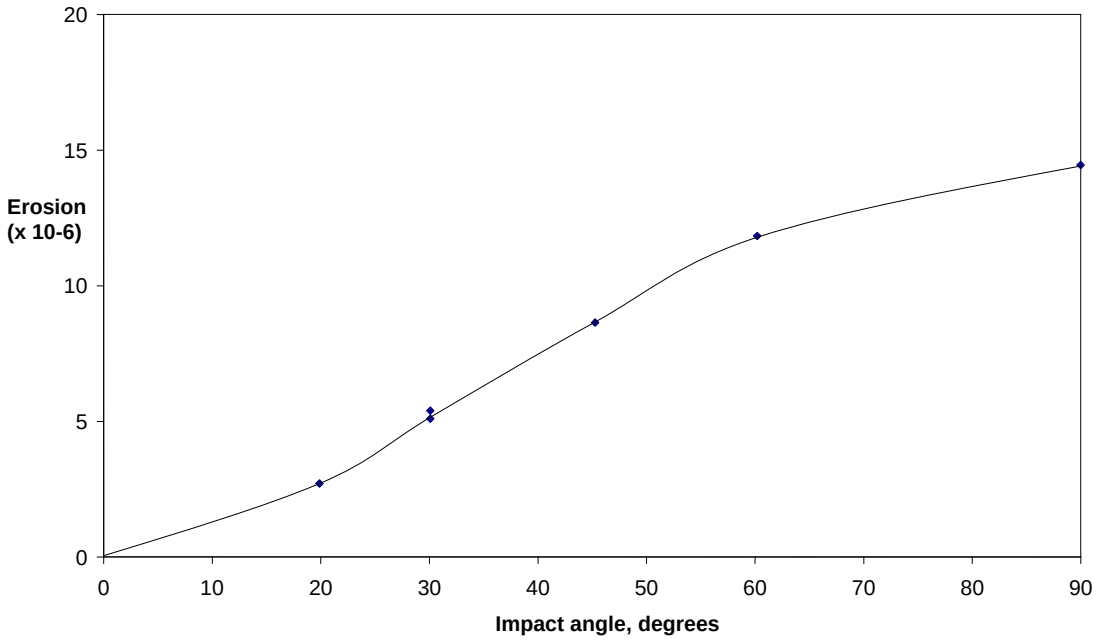

Fig. 9: Erosion vs impingement angle for crushed glass particles (erodent size 140/160 mesh i.e. 95/105 μm) at 55 ms^{-1} [8]

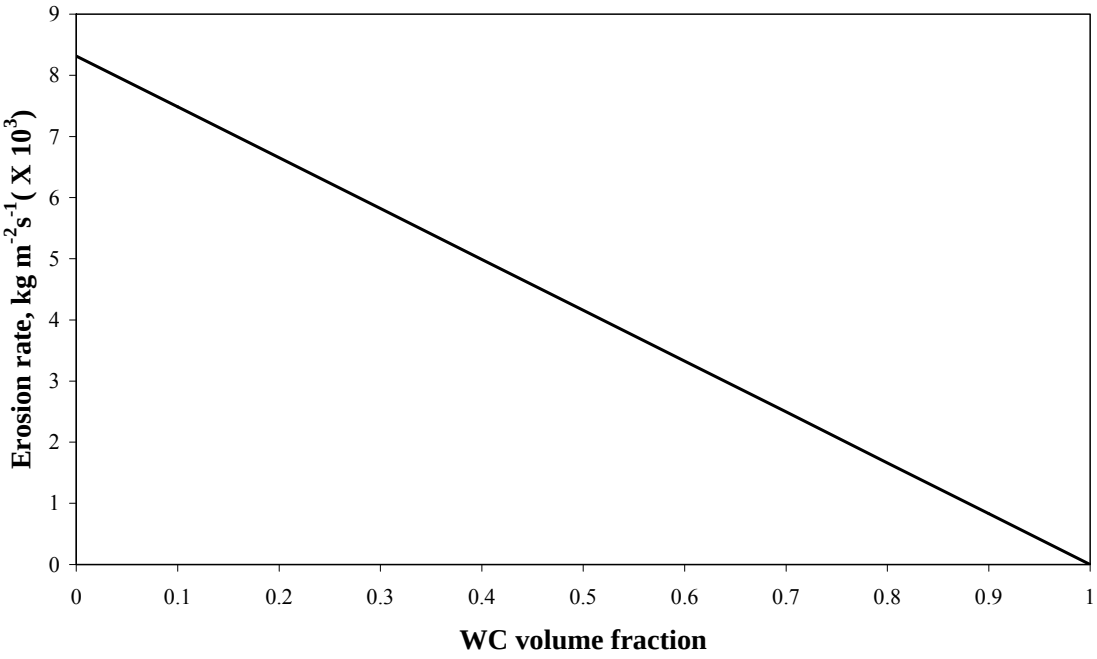

Fig. 10: Predicted erosion rate versus volume fraction trend for the CO-WC cermet at 10 ms^{-1} and at impact angle of 90^{o}

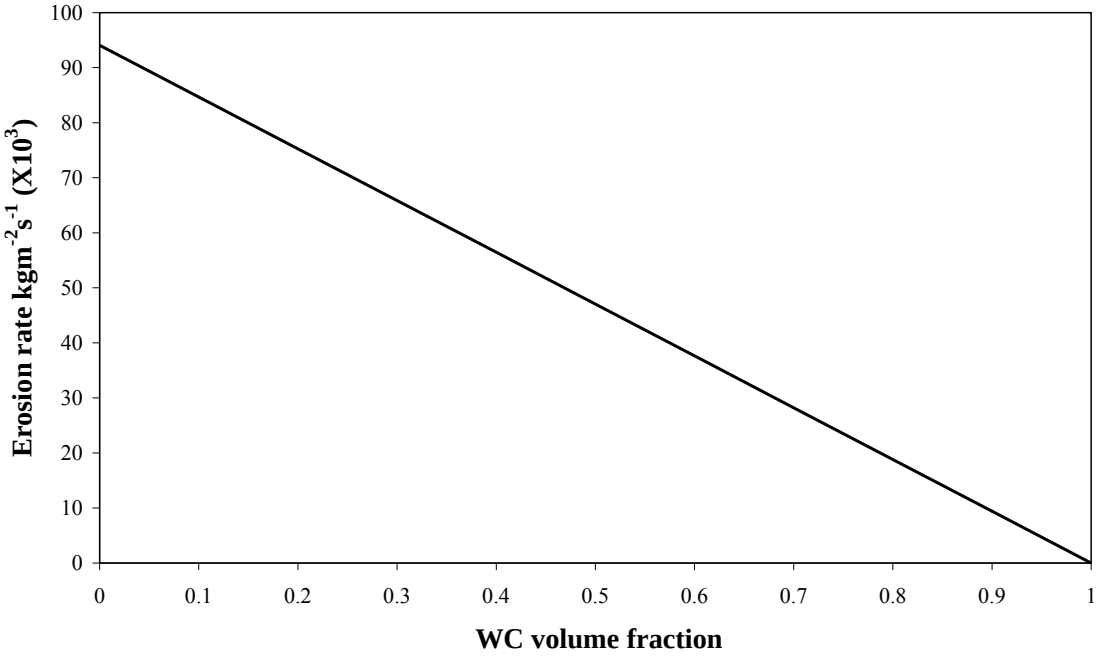

Fig. 11: Predicted erosion rate versus volume fraction trend for the Co-WC cermet at 20 ms^{-1} and at impact angle of 90^o

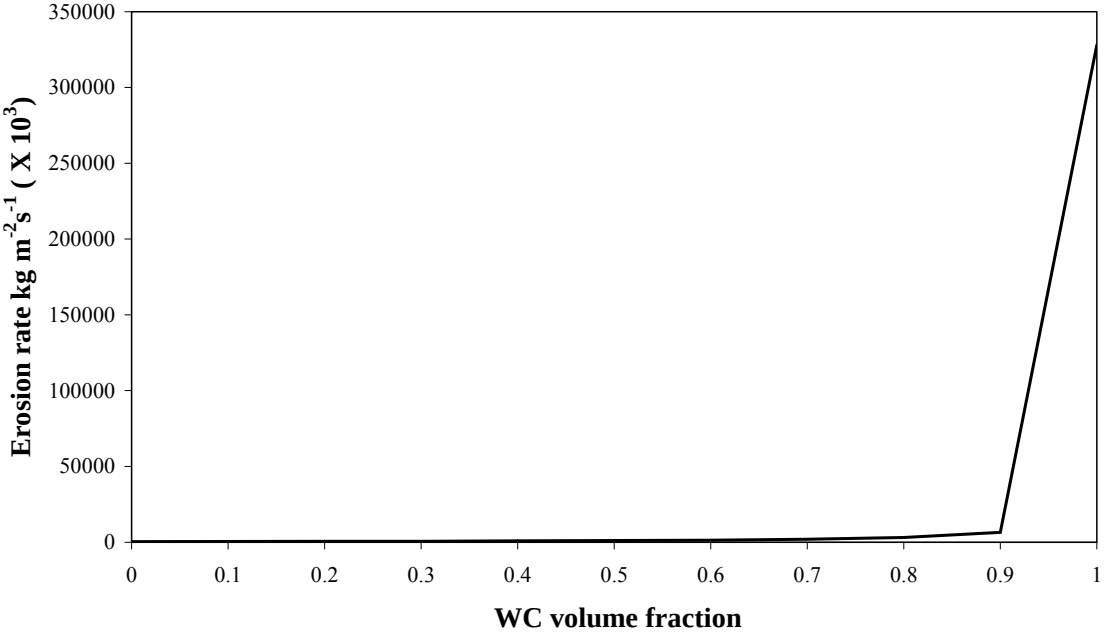

Fig. 12: Predicted erosion rate versus volume fraction trend for the Co-WC cermet at 30 ms^{-1} and at impact angle of 90^o

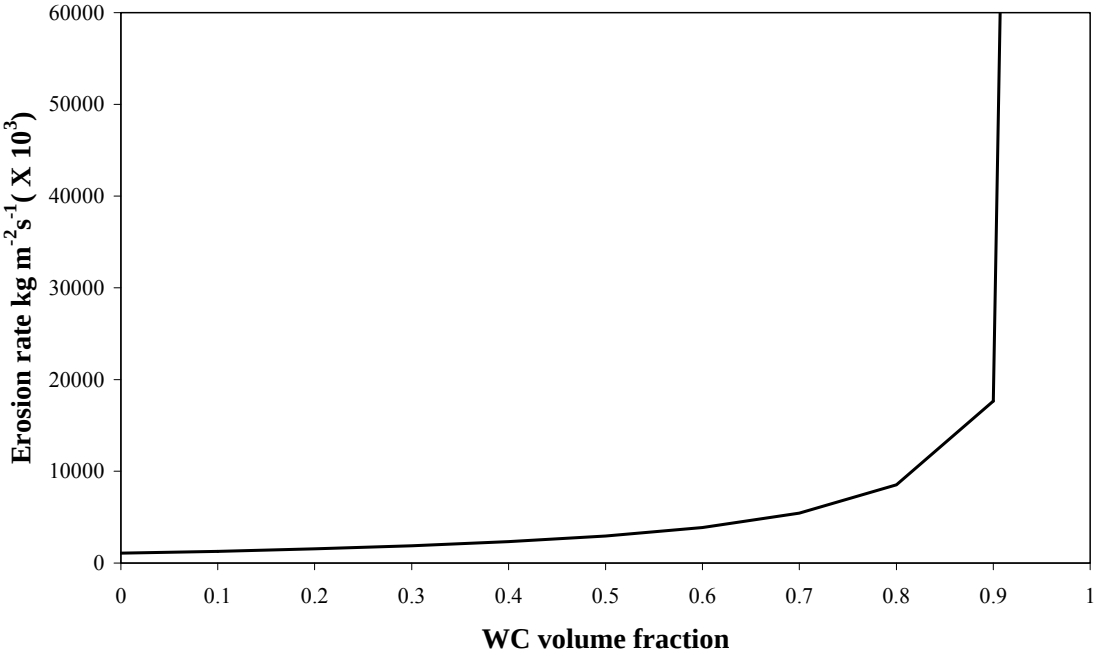

Fig. 13: Predicted erosion rate versus volume fraction trend for the Co-WC cermet at 40 ms^{-1} and at impact angle of 90^o

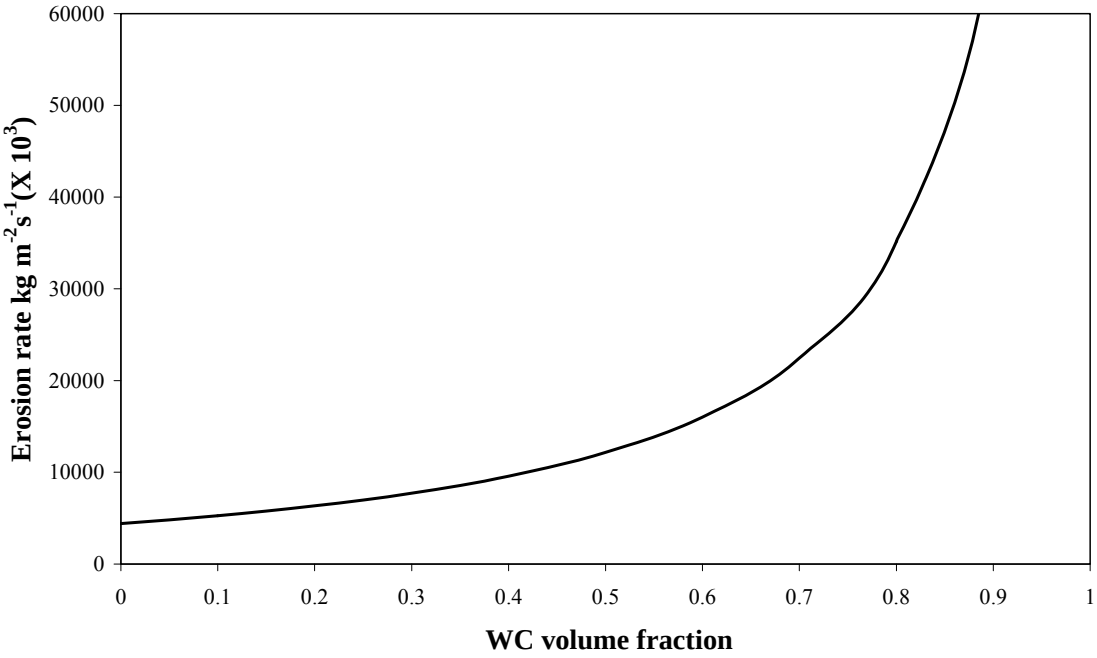

Fig. 14: Predicted erosion rate versus volume fraction trend for the Co-WC cermet at 60 ms^{-1} and at impact angle of 90^o